Received: 26 June 2025 | Revised: 12 September 2025 | Accepted: 11 November 2025 | Published online: 2 December 2025

RESEARCH ARTICLE

Journal of Optics and Photonics Research
2025, Vol. 00(00) 1–14
DOI: 10.47852/bonviewJOPR52026594

BON VIEW PUBLISHING

Remaining Life Estimation of Power Towers Using Strain Sensor Data and LSTM Sequence to Sequence Models

Yu Shi[1], Abolghassem Zabihollah[2,*], Yao-Chi Yu[1], Arunima Pathak[1] and Oluwaseyi Oyetunji[2]

[1] *Department of Mathematics, Tarleton State University, USA*

[2] *Department of Mechanical, Environmental, and Civil Engineering, Tarleton State University, USA*

Abstract: This study investigates the effectiveness of embedding fiber Bragg grating (FBG) sensors in power transmission towers to assess the remaining service life of the structures following impacts from strong winds and hurricanes. FBG sensors monitor the structural integrity of the tower using online measurement of strain variations at critical structural points. The novelty of this work lies in employing a compact long short-term memory (LSTM) framework to estimate the remaining useful lifetime (RUL) from real-time FBG sensor data under both stable and fluctuating wind conditions. To estimate RUL of the tower, LSTM neural network has been implemented, providing predictive insights for proactive maintenance and risk mitigation. A prototype transmission tower was built and experimentally evaluated in a wind tunnel to assess the effectiveness and performance of the proposed RUL model. To simulate different hurricane categories, the experiment was conducted across wind speeds between 0 and 150 mph. FBG sensors installed at critical locations continuously captured real-time strain data, which was transmitted via a low-power micro FBG interrogator to a computer for input into the RUL prediction model. The proposed three-layer LSTM converges rapidly, reducing training and validation loss by nearly two orders of magnitude within 40 epochs, and achieves robust RUL predictions with an average bias of about 50 s on the test set. To quantify structural health, a mathematical health indicator was formulated based on the observed strain responses. The FBG sensors demonstrated high effectiveness in accurately detecting strain variations and monitoring the tower's dynamic behavior under extreme wind loads. The findings support the implementation of condition-based maintenance strategies, enhance safety assessments, and enable early failure detection. This approach not only improves operational reliability but also facilitates timely intervention and maintenance during critical events.

Keywords: power transmission tower, extreme wind events, fiber Bragg grating sensors, structural stability, remaining useful life, LSTM neural network

1. Introduction

The reliability of the power transmission network is essential to modern society, making the structural health of its infrastructure a critical priority. Transmission towers play a central role in ensuring a stable and secure electricity supply across wide regions. However, these structures are exposed to a range of loading conditions, including wind, ice, seismic activity, and dynamic forces from transmission line operations. In coastal regions, hurricanes pose a particularly severe threat, with high winds and storm surges capable of severely damaging or disabling towers. Structural dynamic analysis is therefore crucial to evaluate and maintain the safety and resilience of these vital components. Each year, thousands of transmission towers collapse due to strong winds, leading to significant economic losses and widespread disruptions in power delivery [1]. For example, analyses of recent hurricanes in Florida show storm-induced infrastructure failures, including power transmission system damage, which have inflicted economic losses in the tens of billions [2]. Therefore, timely assessment of the structural integrity and reliability of power transmission infrastructure is a critical factor in minimizing damage to the electrical system caused by hurricanes and strong winds. Given that climate change is projected to increase the frequency and intensity of hurricanes, tornadoes, and downbursts, the need for an accurate and efficient strategy for assessing infrastructure failure risk becomes even more critical [3].

The Saffir–Simpson Hurricane Wind Scale, which classifies hurricanes based on wind speed, is frequently employed in evaluating structural risk [4]. Table 1 shows the scaling of hurricane categories according to this system. To mitigate structural failure and estimate the level of structural safety, researchers and engineers increasingly focus on structural health monitoring (SHM) systems [5]. SHM enables real-time evaluation of structural integrity and early detection of damage in buildings [6], offshore structures [7], bridges [8], and other civil infrastructures. The performance of SHM systems relies heavily on sensor selection, measurement strategies, and optimal sensor placement within the structure [9–11].

Real-time strain measurement is particularly effective for evaluating tower stability, as structural vibration response correlates directly with deformation in structural elements. Traditional

***Corresponding author:** Abolghassem Zabihollah, Department of Mechanical, Environmental, and Civil Engineering, Tarleton State University, USA. Email: azabihollah@tarleton.edu

Table 1
Saffir–Simpson Hurricane categories

Category 1	Wind measured: 50–60 mph Potential Impact: Expect some damage from very hazardous winds.
Category 2	Wind measured: 60–90 mph Potential Impact: Extremely dangerous winds will cause widespread and extensive damage.
Category 3	Wind measured: 90–110 mph Potential Impact: Devastating damage is certain to occur.
Category 4	Wind measured: 110–140 mph Potential Impact: Catastrophic damage will be widespread.
Category 5	Wind measured: 140 mph or higher Potential Impact: Expect catastrophic and widespread destruction

electrical strain gauges, although widely used, require careful wiring, surface bonding, and are susceptible to electromagnetic interference. In contrast, fiber Bragg grating (FBG) sensors offer advantages such as corrosion resistance, electromagnetic immunity, and high sensitivity, making them suitable for continuous monitoring in harsh environments. FBG sensors have been applied in concrete structures [12], road pavements [13], agricultural structures, multi-story buildings, and residential timber buildings [14].

Beyond technical implementation, SHM functionality relies on data analysis and reporting, which are critical for decision-making and assessing structural safety, particularly after hurricane impacts. Wu et al. [15] employed failure mMode and effects analysis to identify potential failure mechanisms in CFRP-packaged FBG sensors, assigning risk priority numbers (RPNs) to evaluate severity and likelihood. Such reliability assessments are broadly applicable across civil engineering domains [16].

A primary goal of SHM is to estimate the remaining useful life (RUL) of structural components under extreme events. Neural network-based algorithms have been widely used for damage estimation. Sequence models, including recurrent neural networks (RNNs) and long short-term memory (LSTM) networks, effectively capture structural dynamics and temporal dependencies [17–19]. Physics-guided learning has proven valuable when data are sparse or noisy; for instance, Al-Adly and Kripakaran [20] developed a physics-informed neural network (PINN) incorporating Kirchhoff–Love plate theory, improving identifiability and prediction accuracy from limited measurements.

Recent research demonstrates LSTM's success across diverse infrastructure monitoring tasks, such as shape control of steel trusses during incremental launching [21], bridge deterioration prediction [22, 23], and damage classification in high-rise buildings [24]. LSTM models also effectively reconstruct missing or corrupted SHM data: Ba et al. [25] recover monitored stress signals and analyze accuracy under varying data loss rates. Foundational work by Hochreiter and Schmidhuber [26] established LSTM as a solution to the vanishing gradient problem, while Elman [27] first introduced the feedback architecture for RNNs, enabling sequential data processing.

The potential of LSTM in vibration-based damage detection and dynamic monitoring has been further reviewed by Avci et al. [28]. Additional innovations include fuzzy-control strategies integrated with LSTM for intelligent structures in seismic zones [29]. Liu et al. [30] propose an improved LSTM that captures the mechanical response under component failure in cable-truss structures, demonstrating accurate failure analysis and practical utility for SHM decision-making. Complementing our use of FBG sensing, Smailov et al. [31] review fibreoptic sensors for concrete structures—covering modeling, deployment, and performance—which supports pairing optical sensing with learning-based monitoring frameworks. Zabihollah and Shi [32] developed multilayered LSTM frameworks integrated with FBG sensors to estimate the RUL of hurricane-exposed buildings.

Other foundational studies support this research, including sensor placement optimization, reliability evaluation of FBG sensors, SHM data repair, and classical modeling approaches such as finite element analysis. Guidelines for wind-load provisions provide parameters for simulating hurricane impacts on structures, and computational models for health monitoring of storage tanks demonstrate the applicability of FBG sensors.

Despite these advances, limited research exists on using LSTM combined with FBG sensors for power transmission towers under hurricane loading. This study addresses this gap by deploying multi-channel FBG sensors to acquire real-time strain data from transmission towers and applying advanced LSTM-based models to predict their RUL under hurricane-induced stresses. Integrating robust sensing technology with predictive AI models aim to enhance the reliability, adaptability, and sustainability of critical power transmission infrastructure.

2. Simulating a Tower Integrated with FBG Sensors

2.1. Dynamic modeling of tower

The structural integrity of a building can be evaluated by precisely determining the stress developed in critical components in real time. Due to the presence of a huge number element withing a tower structure, analysis of the sch structure is performed using numerical approaches, mainly finite element method (FEM). For details of the FEM method for structural analysis, one may consult the book written by Reddy [33].

A typical tower structure can be modeled as a frame structure (Figure 1), consisting of multiple two-node elements. Each node, in the local coordinate system, possesses five DOF: translations along the x, y, and z axes and rotations about the y and z axes. For a frame element, the primary stress occurs along its longitudinal axis and is given by

$$\sigma_x = E\varepsilon_x \tag{1}$$

Figure 1
Finite element simulation of a power transmission tower

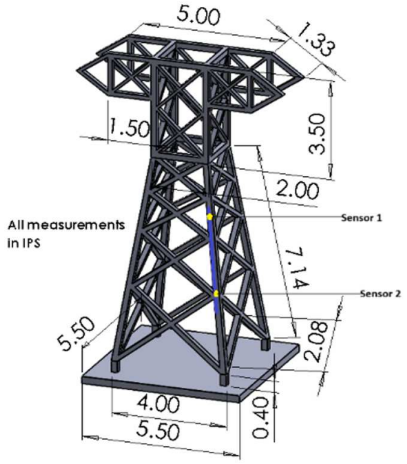

As given in Equation (1), stress (σ_x) is directly proportional to strain (ε_x) by a constant factor of modulus of elasticity (E). Thus, precise strain measurement enables accurate estimation of stress in structural components. The following section outlines the procedure for detecting strain within the tower's structural elements. The dynamic equation for the frame structure can be written as

$$[M]\{\ddot{d}\} + [D]\{\dot{d}\} + [K]\{d\} = \{F(t)\} \tag{2}$$

The matrices M, D, and K represent the mass, structural damping, and stiffness matrices, respectively. For brevity, the explicit details of the element matrices are omitted here. For a comprehensive explanation of the finite element methodology, the reader is referred to Reddy's work. The displacement vector $\{d\}$ comprises the nodal degrees of freedom (DOFs) of the elements, including translations (u, v, w, θ_y, and θ_z) of the element.

The lateral deflection of the beam is determined by $v = Nd$, where based on Euler-Bernoulli beam theory, the shape functions N are determined as

$$N_1 = 1 - 3\frac{x^2}{l^2} + 2\frac{x^3}{l^3},\ N_2 = -x + 2\frac{x^2}{l} - \frac{x^3}{l^2},\ N_3 = 3\left(\frac{x}{l}\right)^2 - 2\left(\frac{x}{l}\right)^3,\ N_4 = \frac{x^2}{l} - \frac{x^3}{l^2} \tag{3}$$

where l is the length of the beam element. The induced axial strain in the beam is determined as

$$\varepsilon_x = -y\frac{d^2N}{dx^2}d \tag{4}$$

Here, y indicates the distance from the neutral axis of the element to the outer surface.

For stability analysis of the structure subjected to hurricane's load, the force vector $\{f(t)\}$ is calculated using Equation (2) as

$$F(t)_{wind} = P_{wind}A \tag{5}$$

where A represents the surface area exposed to the windward side, and the pressure results from wind impact, $P_{Wind,}$ is determined as

$$P_{wind} = C_p\left(\frac{1}{2}\rho_{air}V_{wind}^2\right) \tag{6}$$

where ρ_{air}, C_p are density of air, and shape coefficient of the tower faces the wind. The mean wind speed, V_{wind} altitude-dependent variations can be obtained through the exponential wind profile equation [34]:

$$V_{wind} = V_{10}\left(\frac{H}{10}\right)^{\alpha} \tag{7}$$

where V_{10} is the basic wind speed representing the mean wind speed of 10 min at the altitude of 10 m, H is the altitude, and α is the ground roughness coefficient.

2.2. Strain measurement using FBG sensors

As outlined in Section 2.1, structural stability can be assessed through precise measurement of strain in structural elements subjected to external loads. In this study, fiber Bragg grating sensors are embedded at critical locations to monitor strain changes due to changing the loading and/or structural conditions. The FBGs measure the shift in the reflected light wavelength in response to strain or temperature changes. The peak reflectivity that occurs at the Bragg wavelength is given by the following equation:

$$\Delta\lambda = 2n_{eff}\tau_{FBG} \tag{8}$$

where n_{eff} is the effective refractive index of the mode propagating in the fiber and $_{\text{FBG}}$ indicates the FBG period. Change of wavelength can be determined as

$$\Delta\lambda = \alpha\Delta T + \beta\Delta\varepsilon \tag{9}$$

where α and β indicate the relation of changing wavelength to strain and temperature, respectively. Considering a constant temperature, especially in laboratory conditions, the change in wavelength is only a function of changing strain. Therefore, measuring change of wavelength can be used to measure the strain. For further information on modeling FBG sensors for strain measurement, refer to Reference [35].

3. Prognostic Assessment of Remaining Useful Life Using LSTM Networks

Structural damage and reduced reliability in infrastructure are mainly caused by the buildup of strain, both on the surface and within the materials. To accurately assess structural condition and predict RUL, it's essential to measure cumulative strain and develop reliable health indicators (HIs). In this study, ε_t represents the strain measured at time t. However, predicting strain at the interface between the asphalt surface and the cement-treated base is difficult due to many design factors and uncertainties. Additionally, the random nature of loads, environmental changes, and material differences make it hard to create exact mathematical models for strain behavior. Because of these challenges, combining deep learning and big data in SHM, and RUL prediction has significantly improved our ability to monitor and maintain critical infrastructure.

3.1. Defining failure time based on structural theory

For structural health management, the RUL determines the duration a structure can operate before complete failure, its mathematical formulation at a given time t is expressed as follows:

$$RUL(t) = Curr_{time} - fail_{time} \tag{10}$$

Based on principles of structural mechanics and Hooke's Law, failure is linked to the moment when the material reaches its maximum strain, resulting in loosening or deterioration. Accordingly, the time to failure can be defined as the point at which this maximum strain occurs:

$$fail_{time} = time_{index}(max\ strain) \tag{11}$$

Given that the sensor reads the present time t, the RUL at t is computed via Equation (10).

In addition, the strain undergone by the material can be denoted by ε_t, at any time point t, can be continuously monitored and read from sensors. So, the cumulative strain reflecting the total accumulated deformation over time can also be summarized as

$$Cumu(\varepsilon_t) = \sum_{j=0}^{t} \varepsilon_j \tag{12}$$

By integrating sensor data and structural mechanics principles, we can establish a robust foundation for RUL prediction based on cumulative strain.

Given the relationship between cumulative strain and RUL, machine learning techniques can be employed to develop predictive models. In this study, the raw strain stream gathered from the FBG sensor during the constant wind tunnel experiment (11,083 samples) was first auto-trimmed at the time index, where the peak surface strain was observed. This left 9,839 consecutive records from 0 s to 1,613 s that describe the full degradation path up to failure. For each record, we integrate the shifted strain to obtain a single handcrafted feature, the cumulative strain $Cumu(\varepsilon_t)$, while the target variable Y is $RUL(t)$ derived from Equation (10).

After a logarithmic variance stabilizing transform on RUL and independent min–max scaling of the feature and target, the processed series form a vector of size $\mathbb{R}^{9,839\times 1}$ and label vector of size $\mathbb{R}^{9,839\times 1}$. These data are split chronologically into 80% training/validation and 20% testing windows using a 30-step look back with a stride of 15 samples.

3.2. LSTM networks architecture and mathematical functionality

Since cumulative degradation increases over time, an LSTM recurrent neural network can be employed to predict the RUL of building structures. This method takes advantage of the LSTM architecture's ability to capture long-term dependencies and temporal patterns in sequential data, making it well-suited for modeling structural degradation over time.

Figure 2
A simple RNN network

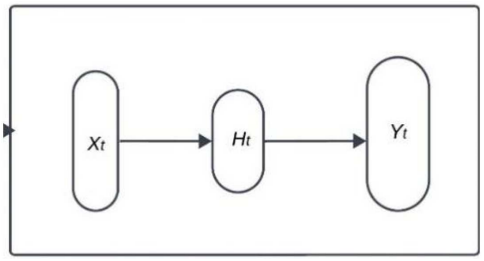

In a basic RNN architecture, as shown in Figure 2, the input at each time step t, denoted as X_t, represents the current information relevant to that moment. Like logistic regression, X_t is multiplied by a weight matrix W_{ht} to transform the input into a hidden state representation. This transformation extracts key features from the input and maps them into a higher-dimensional space, allowing the network to capture complex patterns. The result, $X_t W_{ht}$, is then passed through a nonlinear activation function such as sigmoid or ReLU to produce the hidden state H_t. This nonlinearity enables the model to learn nonlinear dependencies common in real-world data. The hidden state H_t is then combined with another weight matrix W_{ot} to produce the output Y_t, representing the network's prediction or classification at time t. Thus, the output of an RNN at each time step is computed as

$$Y_t = \sigma(W_{ot}H_t + b_Y), \tag{13}$$

where σ is the activation function that is aimed at transforming the weighted sum of the hidden units into the final output? In addition, the formula of hidden unit at time t is expressed as in an LSTM network can be expressed as a function of the current input, the previous hidden state, and a nonlinear activation function:

$$H_t = \delta(W_{ht}X_t + U_tH_{t-1} + b_H). \tag{14}$$

The weight matrix W_{ht} connects the input to the hidden unit, while U_t is another weight matrix that represents the weight at the previous at time step t-1 and connects to the previous hidden unit H_{t-1} from the previous block. Therefore, the functional relationship between X_t and Y_t will be following:

$$Y_t = \sigma(W_{ot}\,\delta(W_{ht}X_t + U_tH_{t-1} + b_H) + b_Y) \tag{15}$$

Both σ, δ represent activation functions, which introduce nonlinearity into the network. Typical activation options are the sigmoid, linear, ReLU, and tanh functions.

RNNs update information at each time step using weight and bias matrices, with gradients propagated through the sequence via the chain rule. However, a key limitation of standard RNNs is the vanishing gradient problem, which hampers the training of deep or long-sequence models by causing gradients to shrink exponentially during backpropagation. To overcome this, Hochreiter and Schmidhuber [26] introduced a new architecture that captures both short-term and long-term dependencies in sequential data, addressing the shortcomings of traditional gradient-based approaches. Originally developed for natural language processing, this architecture, known as LSTM, has since been widely applied to numerical tasks involving regression and classification across diverse domains.

LSTMs architecture shown in Figure 3, like RNNs, is composed of sequential units that are designed to pass information and then model time-series data. Therefore, LSTMs address the gradient vanishing problem in traditional RNNs method. Vanilla-type LSTM unit is a basic and commonly used form of LSTM network and shares some components with an RNN unit but with additional elements to process information flow over time. A vanilla LSTM unit comprises the signals X_t, $H_t$and C_t, with information flow controlled by three gates: $f^{(t)}$(forget), $i^{(t)}$ (input), and $o^{(t)}$ (output).

The input and forget gates in an LSTM network use sigmoid activation functions to selectively regulate which information is retained or discarded as it flows through the network.

Figure 3
A vanilla LSTM unit

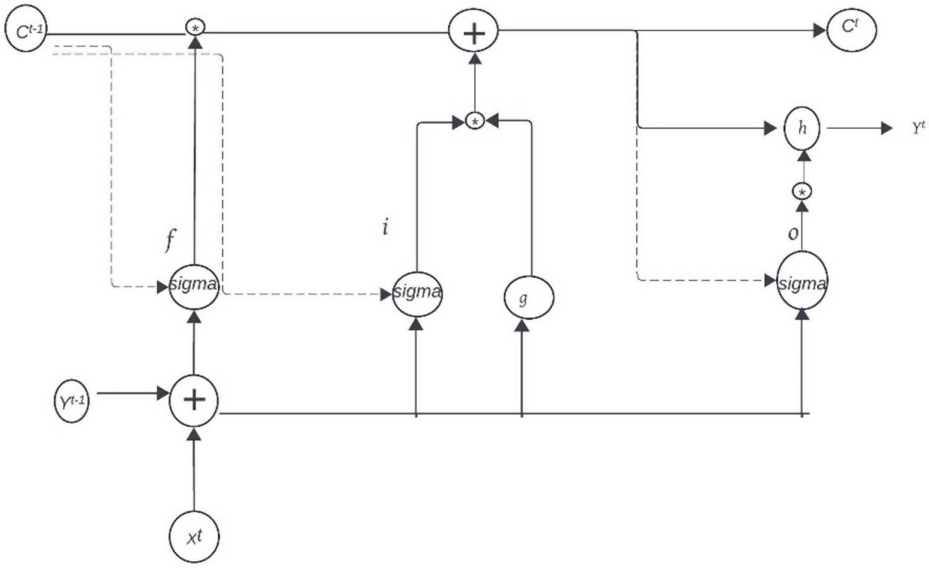

The input gate determines which aspects of current input information X_t, previous Y_{t-1} and the previous cell state C_{t-1} are relevant to updating the cell state by a sigma function. Therefore, the formula of input gate can be expressed as

$$i^{(t)} = \sigma(W_i X_t + U_i Y_{t-1} + V_i \odot C_{t-1} + b_i) \tag{16}$$

Conversely, using a σ activation function on X_t and Y_{t-1}, the forget gate yields $f^{(t)}$, which determines the proportion of C_{t-1} kept versus discarded. Hence, the expression for the forget gate is

$$f^{(t)} = \sigma\left(W_f X_t + U_f Y_{t-1} + V_f \odot C_{t-1} + b_f\right) \tag{17}$$

Furthermore, the output gate can be represented using the following formula:

$$o^{(t)} = \sigma(W_o X_t + U_o Y_{t-1} + V_o \odot C_{t-1} + b_o) \tag{18}$$

Referring to the above three formulations, it is obvious that the updated information within an LSTM unit is governed by point-wise multiplication $\odot$ and weight matrices W, U, and V, alongside a constant bias b. In the input gate, the three weight matrices function to filter the incoming data and determine which information should be retained for the next time step. Conversely, in the forget gate, these matrices are structured to eliminate irrelevant or unnecessary information. This selective mechanism of the input and forget gates allows the LSTM unit to effectively discard redundant data from the previous cell state, ensuring that only essential and meaningful information is preserved for updating the state of the subsequent unit. This selective retention allows the network to avoid the necessity of preserving all information from the initial stages to the final output, thereby mitigating the gradient vanishing issue commonly encountered in RNN chain structures. This capability is crucial for processing sequential data with long-range dependencies.

In addition, the cell state is a key component of LSTM architecture; it facilitates the transmission of information across numerous time steps with minimal alteration. This mechanism contributes to the preservation of long-term dependencies within the sequence, effectively addressing the vanishing gradient problem that plagues standard RNNs. The cell state at time t is given by regulated inputs and forget gates that

$$c^{(t)} = z^{(t)} \bigodot i^{(t)} + c^{(t-1)} \bigodot f^{(t)} \tag{19}$$

and $z^{(t)} = g(W_z X_t + U_z Y_{t-1} + b_z)$ is referred to as the block input.

Finally, the output predictions derived via the LSTM architecture will be the point-wise multiplication of current cell state with the output gate that

$$Y_t = g\left(c^{(t)}\right) \bigodot o^{(t)} \tag{20}$$

Using all prior time steps, the model outputs the next target value Y_t.

In the proposed sequence-to-sequence framework, the scalar input at each time step is the cumulative strain denoted as $X_t = Cumu(\varepsilon_t)$; the corresponding label is the log-transformed remaining useful life, given by $Y_t = \log(1 + \mathrm{RUL}(t))$. Learning the mapping is achieved through a three-layer LSTM encoder $X_{t-29} \mapsto Y_t$ through end-to-end optimization of its weight matrices and biases. To emphasize accuracy near structural failure, the loss function is re-weighted so that samples drawn from the final 30% of the life curve receive a threefold penalty during training.

4. Experimental Work

4.1. Modeling

It is understood that in real applications, transmission towers are made from steel. However, due to the limitation of making a prototype using steel for experimental works in the laboratory, the current research work is performed on a 3D-printed stower. It is worth noting that the range of allowable strain for steel structural members is around 0.1% while for current 3D-printed tower could be up to 3%. Therefore, a truss structure, as shown in Figure 4(a) was modeled in SolidWorks and converted to stereolithographic

Figure 4
Finite element modeling of a power transmission tower: (a) 3D model and (b) 3D printed tower

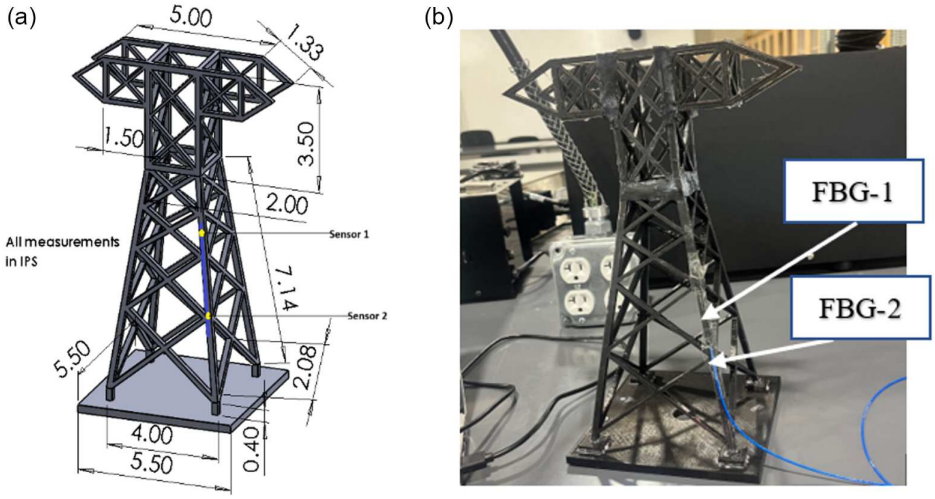

format (STL) and imported into the Flash Print 3D printer application for slicing and sending the G-codes to the printer. Modulus of elasticity of the 3D-prinetd beam is assumed as 2 GPa. An array of FBG sensors is connected to one of the main columns as shown in Figure 4(b). Figure 4 provides a detailed representation of the power transmission tower, illustrating the geometric configuration and key dimensions utilized in the finite element (FE) model developed for this study. All measurements are presented in the inch-pound-second (IPS) system. This FE model serves as the foundational structural representation, enabling the simulation of realistic loading conditions and the strategic placement of virtual sensors. Notably, the locations of two FBG sensors, designated as FBG 1 and FBG 2, are highlighted on a specific tower leg, indicating the points where strain data were either measured or simulated for the subsequent analysis. This detailed modeling is crucial for understanding the structural behavior and for validating the sensor data used in the remaining life estimation.

In this study, a bare fiberoptic cable (FBG-MR0010, sourced from Micronor Sensors, Inc.) containing four FBG sensors spaced 10 mm apart was employed to measure the induced strain on the chosen frame element. The fiberoptic cable was connected to an FBGX100 Interrogator (FISENS®) operating within a wavelength range of 808–880 nm. The FBG sensors were attached to the outer surface of the column facing the wind load using adhesive tape.

4.2. Wind-tunnel simulation of hurricane-induced tower response

To replicate strong winds and hurricane conditions in the laboratory, a wind tunnel manufactured by Aerolab® was utilized. The strain data captured by the FBG sensors are gathered by an FBG interrogator, which sends optical signals to a computer for real-time visualization. Figure 5 shows a schematic diagram of the experimental setup, including the tower prototype, wind tunnel chamber, wind speed controller, FBG interrogator, and the computer used to display the measured strain.

Figure 6 depicts the experimental arrangement used to measure dynamic strain on the scaled power transmission tower model inside a controlled wind tunnel setting.

Figure 5
Layout of the wind tunnel testing procedure

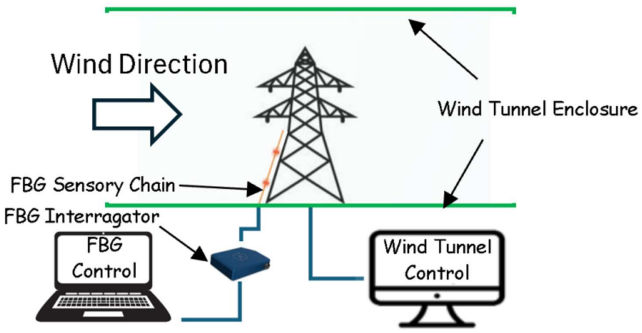

The correlation between the fan speed and the wind speed in the testing area is extracted from the calibration data provided by (aero lab®) as

$$Wind\,speed\ (mph) = 0.062\ Fan\,speed\ (RPM) \quad (21)$$

The image clearly depicts the lattice tower model positioned inside the transparent test section of the wind tunnel, highlighting the method for subjecting the structure to controlled aerodynamic loads. The blue arrow on the image explicitly indicates the direction of airflow, signifying the applied wind forces during the experimental trials. This controlled experimental arrangement was essential for acquiring high-fidelity, time-series strain data, which accurately reflects the dynamic response of the tower model under varying wind speeds. The data obtained from this setup serve as a critical empirical basis for developing and validating the LSTM sequence-to-sequence models utilized in the RUL estimation framework.

5. Results and Discussion

5.1. Numerical strains determination

The induced strains at three distinct locations along the tower elements, as illustrated in Figure 4, were evaluated under various

Figure 6
Tower strain monitoring during wind tunnel testing

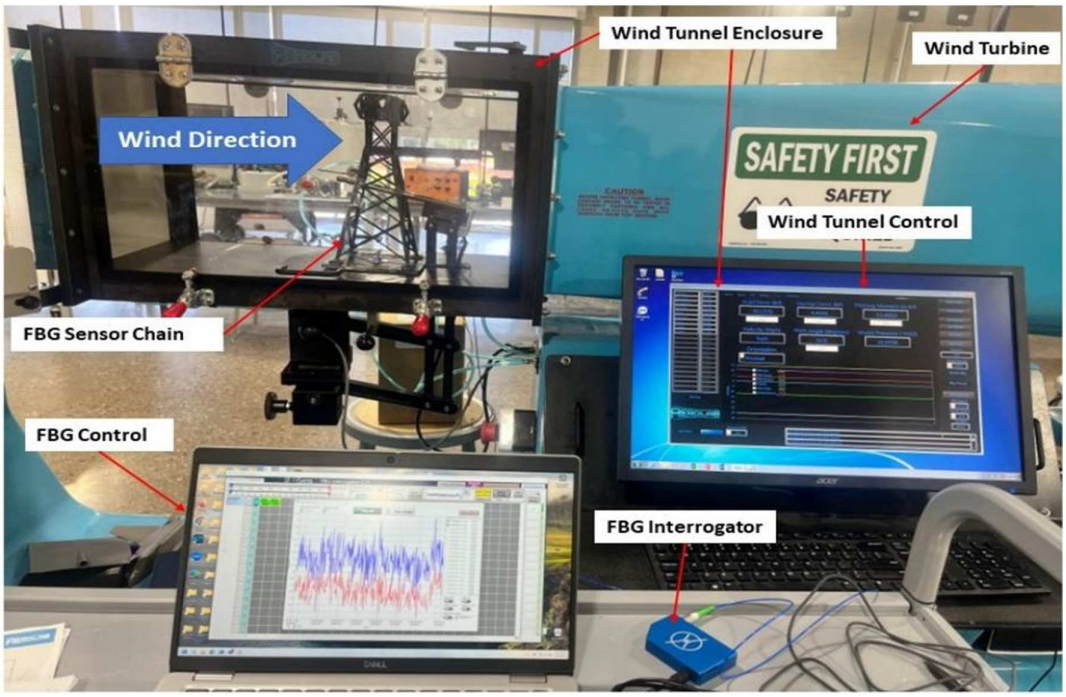

Figure 7
Finite element strain determination for a tower subject to wind, a) 30mph, b) 150 mph

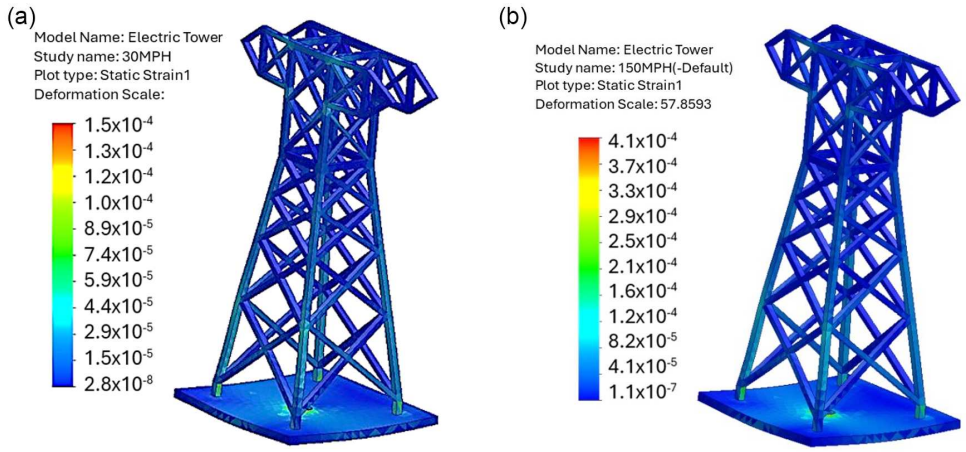

wind speed conditions. The numerical results were obtained using the FEM model described in the Appendix, implemented through the FEM software shown in Figure 7. To ensure accuracy, the support conditions in the model were aligned with those used in the experimental setup. It is important to note that in practical applications, the four corners of the truss are fixed. However, in the current experiment, the truss was fixed only at the midpoint, resulting in the left side lifting off the surface when subjected to wind loading. As anticipated, the induced strain values increased with rising wind speeds, corresponding to the greater wind pressure calculated by Equation (5).

5.2. Experimental strain measurement

To evaluate "the operational behavior and features of the structure embedded with FBG sensors, the tower equipped with these sensors (illustrated in Figure 5) was placed inside a wind tunnel and exposed to varying wind speeds. The wind velocity was controlled by adjusting the fan speed, ranging from 0 to 150 mph. For conciseness, results corresponding to low wind speeds are excluded from the figure since the strain induced at such speeds was minimal. Figure 8 displays the strain responses measured by FBG-1 (blue line) and FBG-2 (red line) at wind speeds between 50 and 60 mph.

Figure 8
FBG-based strain measurements of the tower under hurricane category 1 (50–60 mph)

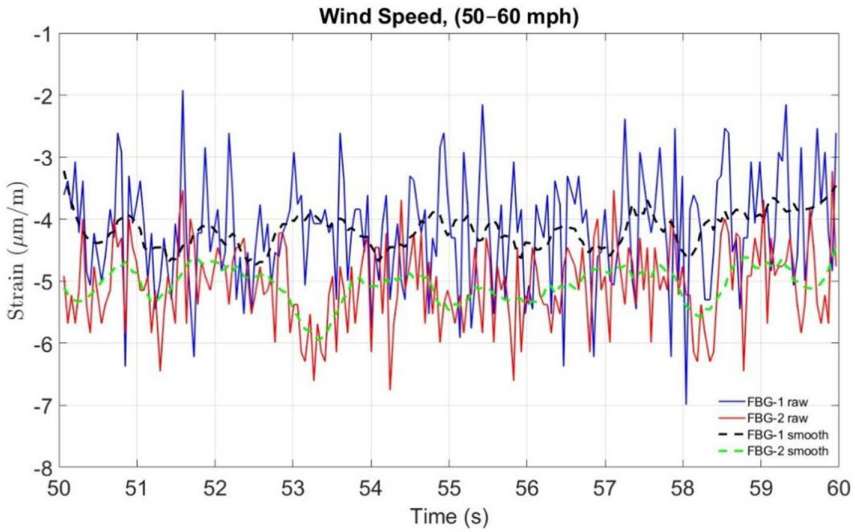

Figure 9
FBG-based strain measurements of the tower under hurricane category 2 (60-90 mph)

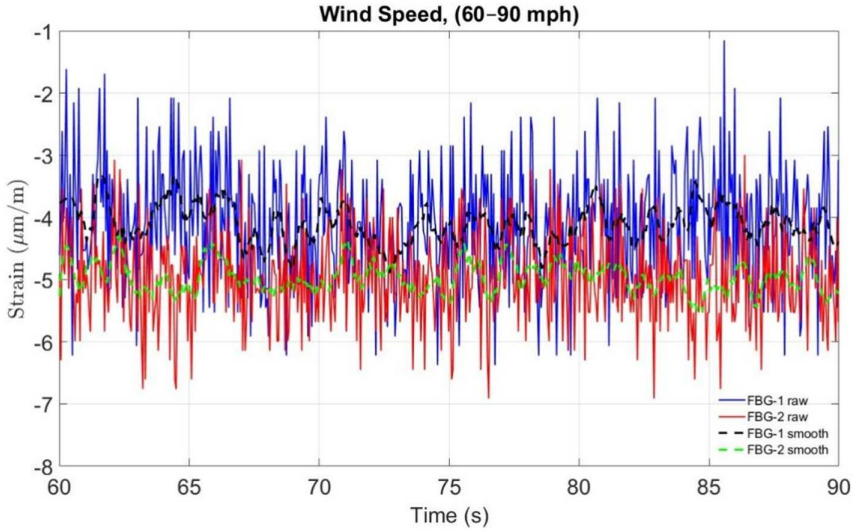

Figure 8 presents the dynamic strain response measured by two fiber Bragg grating sensors, FBG-1 (blue) and FBG-2 (red), over an interval of 300 seconds, starting at about 400 s and ending at 700s under wind speeds ranging from 50 to 60 mph. The y-axis, labeled "Strain (micrometer/m)," quantifies the deformation detected by the sensors. Both sensors exhibit fluctuating strain readings, indicative of the varying forces exerted by the wind. FBG-1 generally registers higher strain values, with its peaks reaching approximately 8–9 micrometer/m, while FBG-2 shows slightly lower magnitudes, typically peaking around 6–7 micrometer/m. A notable characteristic in this wind speed range is the overall lower magnitude of strain compared to higher wind speed conditions and the presence of both positive and negative strain values for FBG-1 at the beginning of the measurement, suggesting initial oscillatory behavior or a settling phase. These data clearly illustrate the dynamic nature of structural response to moderate wind conditions, with both sensors capturing the transient strain variations.

Figure 9 illustrates the strain response measured by FBG-1 (blue) and FBG-2 (red) within a wind speed range of 60 to 90 mph, measured over a duration beginning roughly at 700 s to 900 s. The y-axis represents "Strain (micrometer/m)." As wind speed increases from the previous range, a corresponding increase in the magnitude and variability of the measured strain is evident. FBG-1 consistently records higher strain values than FBG-2 throughout this interval, with its peaks frequently exceeding 10 micrometer/m. FBG-2, while following similar trends, registers peak strains typically below 8 micrometer/m. These data demonstrate a clear dynamic response to the elevated wind speeds, characterized by more pronounced and rapid fluctuations in strain for both sensors.

Figure 10
FBG-based strain measurements of the tower under hurricane category 3 (90-110 mph)

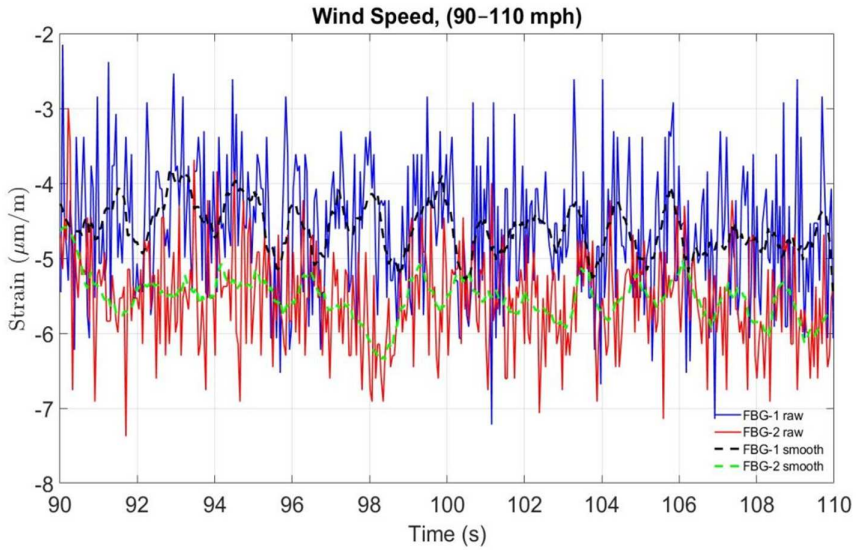

Figure 11
FBG-based strain measurements of the tower under hurricane category 4 (110–140 mph)

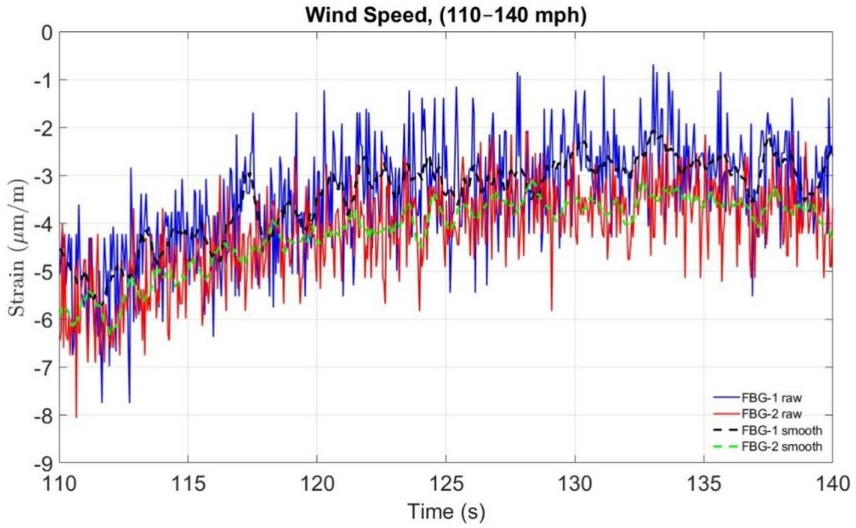

The distinct separation between the strain magnitudes recorded by FBG-1 and FBG-2 suggests different loading distributions or sensor locations on the monitored structure.

Figure 10 displays the strain response from FBG-1 (blue) and FBG-2 (red) during wind speeds ranging from 90 to 110 mph, within a time frame commencing at about 1000 seconds to 1200 s. The y-axis denotes "Strain (micrometer/m)". At these higher wind speeds, both sensors exhibit significantly increased strain magnitudes and more intense fluctuations compared to the previously observed lower wind speed regimes. FBG-1 consistently shows the largest strain values, frequently reaching and exceeding 14 micrometer/m at its peaks. FBG-2 also shows substantial strain, often peaking around 10-12 micrometer/m. The dynamic nature of the strain is highly evident, with rapid and significant excursions from the mean, reflecting the considerable forces imparted by high winds. The persistent offset between the readings of FBG-1 and FBG-2 continues to be observed, indicating either distinct structural responses at their respective locations or inherent sensor characteristics.

Figure 11 presents the strain data for FBG-1 (blue trace) and FBG-2 (red trace) under the most extreme wind conditions, ranging from speeds between 110 and 140 mph, measured near 1200s and 1600 s. The y-axis is labeled "Strain (micrometer/m)". In this severe wind speed range, the measured strain values reach their highest magnitudes across all presented figures, indicative of the maximum loads experienced by the monitored structure. Both FBG-1 and FBG-2 demonstrate highly dynamic and oscillating strain, with FBG-1 consistently showing higher peak strains, frequently surpassing 15 micrometer/m. FBG-2 also exhibits substantial strain, often reaching 12-13 micrometer/m. The pronounced peaks and troughs, along with the overall elevated strain levels, underscore the significant structural response to cyclonic or hurricane-force winds. These data highlight the critical importance of monitoring structural integrity under such

Figure 12
Cumulative strain via time

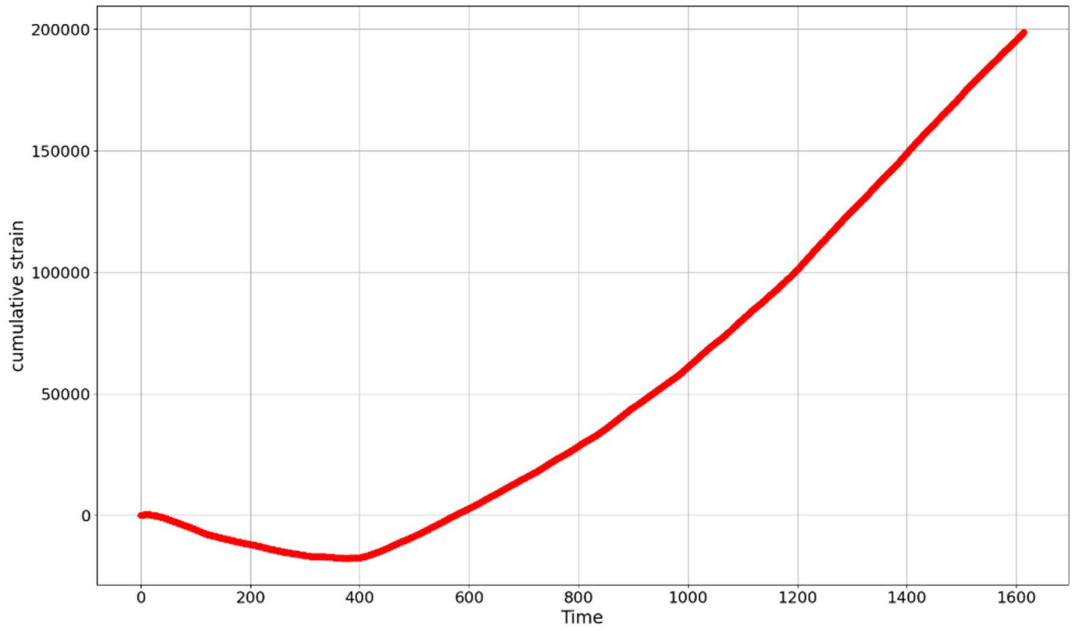

extreme environmental conditions, as the dynamic strain behavior directly correlates with the applied wind loads and potential fatigue accumulation.

6. Training the LSTM and Predictive Results

As outlined in Section 2, this study employs a three-layer LSTM neural network to estimate the RUL of building structures, aiming to proactively mitigate potential damages. This LSTM sequence-to-sequence architecture can capture long-term dependencies in degradation behaviors, which are critical for accurate RUL prediction. In addition, the gated structure of LSTM helps avoid vanishing gradient issues and enables the model to learn both steady and fluctuating wind-induced patterns in structural response data. To enhance the LSTM model's learning parameters, they are fine-tuned to improve predictive accuracy by experiments involving both steady and adjustable wind speed conditions. The data preprocessing and model training tasks were executed in Python version 3.11.5, running on a Windows 11 system powered by an Intel vPRO Essential i5 processor.

Raw strain measurements $\varepsilon(t)$ obtained from the embedded FBG sensors were first truncated at the automatically identified failure index, as detailed in Section 2. To guarantee that all values remained nonnegative, the data were adjusted by shifting them so that $\varepsilon \geq 0$ at each time step. Given that the RUL decreases rapidly near the end of a component's lifespan, a natural logarithmic transformation was applied to stabilize its variance, resulting in the transformed target $y(t) = \log(RUL(t) + 1)$. Both the input feature and the transformed target were independently normalized using min–max scaling to the $[0, 1]$ range.

For sequence learning, we slid a fixed-length window of 30 time steps (≈7.5 s) through the series with a stride of 15 samples. All windows before 80 % of the end-of-life time-line (chronological split) formed the training set; the remaining 20 % were kept strictly for testing. A further 20 % of the training windows were set aside as a validation fold. The predictive core of our framework is a compact three-layer LSTM encoder. Each recurrent tier contains 128 hidden units followed by a 20 % dropout and batch-normalization; the first two layers return their full hidden sequences, while the third outputs only its final state, which is fed to a single linear neuron for the remaining-life estimate. During training, we slide a 30-step window along the sensor stream with a stride of 15 samples, so every labeled example summarizes roughly half a minute of structural response. Batches of 128 windows are processed with the Adam optimizer, whose learning rate follows a cosine-decay-with-restarts schedule with initial learning rate = 5 × 10^-^4 and the first period being 2000 steps. Gradients are clipped to a unit ℓ_2-norm, and a mild weight-decay of 1×10^{-5} acts as further regularization.

To emphasize accuracy near failure, windows lying in the last 30 % of the structure's useful life receive a threefold sample weight. Training stops early if the validation loss fails to improve for ten consecutive epochs, but never exceeds 120 epochs. Finally, we apply a snapshot ensemble: the four best checkpoints are averaged to form the model used for inference, yielding a smoother and more robust RUL trajectory.

The workflow starts by transforming raw FBG-sensor strain readings into a cumulative-strain signal, as shown in Figure 12. By trimming the dataset at the observed point of failure and correcting for negative offsets, the cumulative curve rises quasi-linearly from 0 to ≈ 4.5 × 10^5 m / μm over a 1600 s load sequence, providing a physically meaningful degradation trajectory that is used as the sole input feature. Training converges rapidly, as shown in Figure 13, where both training and validation loss fall by two orders of magnitude within 40 epochs and stabilize near zero, indicating strong generalization and no overfitting. The resulting model delivers a smooth RUL trajectory, as shown by the orange line in Figure 14, that closely follows the ground truth (blue) across the entire test horizon; predictions exhibit a consistent but modest

Figure 13
Evolution of training and validation loss for the LSTM RUL predictor

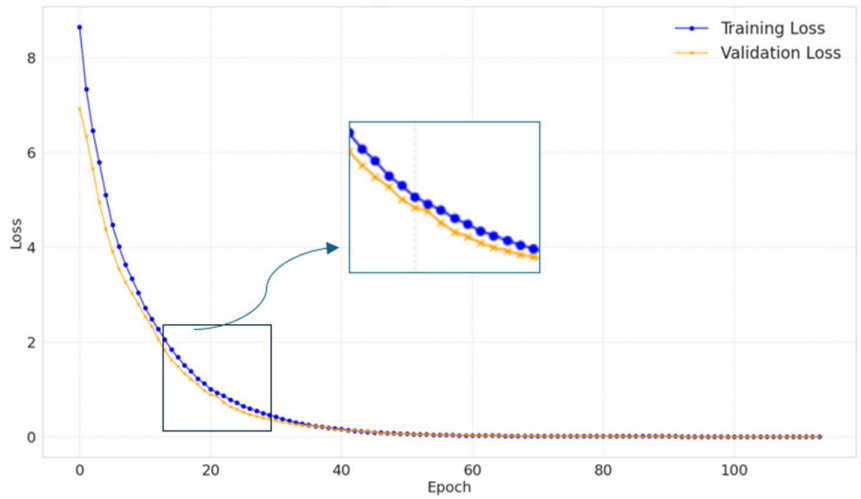

Figure 14
LSTM-based prediction of remaining useful life (RUL) for the real test set

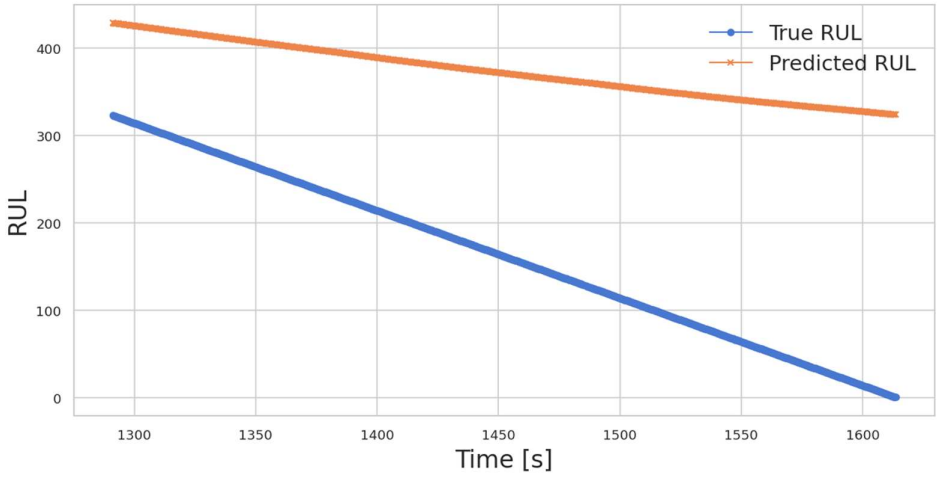

positive bias of ≈ 50 s, confirming that the network captures the monotonic deterioration pattern while erring on the safe side.

7. Conclusion

Failure prediction of power transmission towers subject to wind load and hurricanes has been investigated using surface-mounted FBG sensors located at the critical points of the tower. A scaled-down model of a typical power line transmission tower has been developed in Autodesk Inventor®. The stress analysis has been performed using a simulated wind speed of 150 mph. The scaled-down model of the tower is built for experimental purposes. The prototype model has been placed in a wind tunnel and subjected to a wind speed of approximately 150 mph. The induced strain has been measured using four FBG sensors mounted at the surface of a selected element at critical points. It was legalized that surface-mounted FBG offers a low-cost, safe method to assess the structural integrity of power transmission towers during hurricanes. In the second phase, the RUL of the tower after hitting the hurricane has been estimated using a three-layer LSTM neural network. Strain readings from the FBG system were sufficient to train the model. The LSTM's RUL estimates tracked the tower's true life closely, supplying actionable guidance for timely maintenance and preventive intervention of power outages can be achieved by leveraging knowledge of a tower's RUL. Quantitatively, this LSTM framework reduced training and validation loss by nearly two orders of magnitude within 40 epochs of convergence without overfitting. On the held-out test set, the predicted RUL closely tracked the ground truth with an average bias of approximately 50s, demonstrating both accuracy and robustness under varying wind-induced conditions. Maintenance engineers at power transmission agencies can use RUL estimates to mitigate the risk of structural failures, enhance the safety and reliability of power delivery, and protect lives during extreme weather events such as hurricanes.

Recommendations

We demonstrate that embedded FBG sensing can deliver affordable, high-fidelity structural monitoring in residential settings.

Using the derived reliability model, engineers can estimate safety margins for buildings exposed to strong winds and hurricanes.

The proposed system can be further tailored to accommodate specific local weather conditions and different building types. It is recommended that this reliability-based damage and safety assessment model be adopted by local authorities and insurance agencies for effective risk evaluation and management.

Acknowledgment

The authors wish to thank the support provided by Mayfield College of Engineering and College of Science and Mathematics at Tarleton State University.

Ethical Statement

This study does not contain any studies with human or animal subjects performed by any of the authors.

Conflicts of Interest

The authors declare that they have no conflicts of interest to this work.

Data Availability Statement

Data are available from the corresponding author upon reasonable request.

Author Contribution Statement

Yu Shi: Methodology, software, formal analysis, data curation, writing – original draft, writing – review & editing, visualization, supervision, and project administration. **Abolghassem Zabihollah:** Conceptualization, methodology, software, validation, investigation, resources, data curation, writing – original draft, writing – review & editing, visualization, supervision, and project administration. **Yao-Chi Yu:** Methodology, software, formal analysis, data curation, and writing – original draft. **Arunima Pathak:** Investigation, writing – original draft, and visualization. **Oluwaseyi Oyetunji:** Investigation.

References

[1] Camelo, J., & Mayo, T. (2021). The lasting impacts of the Saffir-Simpson Hurricane Wind Scale on storm surge risk communication: The need for multidisciplinary research in addressing a multidisciplinary challenge. *Weather and Climate Extremes*, *33*, 100335. https://doi.org/10.1016/j.wace.2021.100335

[2] Florida residential wind loss mitigation study. (2008). Applied Research Associates, ARA Final Report 18401, Version 1.11. Retrieved from: https://enclosurenews.com/PDFs/ARA_Loss_Mitigation_Study.pdf

[3] Amirinia, G., & Jung, S. (2017). Buffeting response analysis of offshore wind turbines subjected to hurricanes. *Ocean Engineering*, *141*, 1–11. https://doi.org/10.1016/j.oceaneng.2017.06.005

[4] Abdulkarem, M., Samsudin, K., Rokhani, F. Z., & A Rasid, M. F. (2020). Wireless sensor network for structural health monitoring: A contemporary review of technologies, challenges, and future direction. *Structural Health Monitoring*, *19*(3), 693–735. https://doi.org/10.1177/1475921719854528

[5] Farrar, C. R., & Worden, K. (2007). An introduction to structural health monitoring. *Philosophical Transactions of the Royal Society A: Mathematical, Physical and Engineering Sciences*, *365*(1851), 303–315. https://doi.org/10.1098/rsta.2006.1928

[6] Sivasuriyan, A., Vijayan, D. S., Górski, W., Wodzyński, Ł., Vaverková, M. D., & Koda, E. (2021). Practical implementation of structural health monitoring in multi-story buildings. *Buildings*, *11*(6), 263. https://doi.org/10.3390/buildings11060263

[7] Maraveas, C., & Bartzanas, T. (2021). Sensors for structural health monitoring of agricultural structures. *Sensors*, *21*(1), 314. https://doi.org/10.3390/s21010314

[8] Park, G., & Inman, D. J. (2007). Structural health monitoring using piezoelectric impedance measurements. *Philosophical Transactions of the Royal Society A: Mathematical, Physical and Engineering Sciences*, *365*(1851), 373–392. https://doi.org/10.1098/rsta.2006.1934

[9] Ostachowicz, W., Soman, R., & Malinowski, P. (2019). Optimization of sensor placement for structural health monitoring: A review. *Structural Health Monitoring*, *18*(3), 963–988. https://doi.org/10.1177/1475921719825601

[10] Braunfelds, J., Senkans, U., Skels, P., Janeliukstis, R., Porins, J., Spolitis, S., & Bobrovs, V. (2022). Road pavement structural health monitoring by embedded fiber-Bragg-grating-based optical sensors. *Sensors*, *22*(12), 4581. https://doi.org/10.3390/s22124581

[11] Sliti, M., & Boudriga, N. (2021). Building Structural Health Monitoring: An FBG-based estimation of external vibrations. In *2021 18th International Multi-Conference on Systems, Signals & Devices*, 1026–1031. https://doi.org/10.1109/SSD52085.2021.9429378

[12] Zhou, C., Jia, Z., Song, S., Luo, S., Zhang, X., Zhang, X., . . . , & Pei, X. (2025). Application of FBG sensor in health monitoring of engineering building structure: A review. *Sensor Review*, *45*(1), 129–145. https://doi.org/10.1108/SR-06-2024-0572

[13] Amaya, A., & Sierra-Pérez, J. (2022). Toward a structural health monitoring methodology for concrete structures under dynamic loads using embedded FBG sensors and strain mapping techniques. *Sensors*, *22*(12), 4569. https://doi.org/10.3390/s22124569

[14] Yassin, M. H., Farhat, M. H., Soleimanpour, R., & Nahas, M. (2024). Fiber Bragg grating (FBG)-based sensors: a review of technology and recent applications in structural health monitoring (SHM) of civil engineering structures. *Discover Civil Engineering*, *1*, 151. https://doi.org/10.1007/s44290-024-00141-4

[15] Wu, T., Liu, G., Fu, S., & Xing, F. (2020). Recent progress of fiber-optic sensors for the structural health monitoring of civil infrastructure. *Sensors*, *20*(16), 4517. https://doi.org/10.3390/s20164517

[16] Liu, Z., Li, Y., Zhang, N., Liang, Z., & Li, F. (2021). Reliability analysis of CFRP-packaged FBG sensors using FMEA and FTA techniques. *Applied Sciences*, *11*(22), 10859. https://doi.org/10.3390/app112210859

[17] Zabihollah, A., Hajyalikhani, P., & Vuddandam, R. (2024). Evaluation of embedded FBG sensors for strain monitoring of residential timber buildings under various wind speeds. *Structural Monitoring and Maintenance*, *11*(4), 263–275. https://doi.org/10.12989/SMM.2024.11.4.263

[18] Richter, B., Herbers, M., & Marx, S. (2024). Crack monitoring on concrete structures with distributed fiber optic sensors—Toward automated data evaluation and assessment.

Structural Concrete, *25*(2), 1465–1480. https://doi.org/10.1002/suco.202300100

[19] Zhao, Z., & Zhang, H. (2024). An automatic analysis approach of bridge life based on engineering mathematics and LSTM. In *2024 19th Annual System of Systems Engineering Conference*, 308–313. https://doi.org/10.1109/SOSE62659.2024.10620948

[20] Al-Adly, A. I. F., & Kripakaran, P. (2024). Physics-informed neural networks for structural health monitoring: A case study for Kirchhoff–Love plates. *Data-Centric Engineering*, *5*, e6. https://doi.org/10.1017/dce.2024.4

[21] Hu, Z., Chen, H., Dong, C., Li, Q., & Wang, R. (2025). LSTM-based prediction method for shape error of steel truss during incremental launching construction. *PLOS One*, *20*(7), e0324932. https://doi.org/10.1371/journal.pone.0324932

[22] Miao, P., Yokota, H., & Zhang, Y. (2023). Deterioration prediction of existing concrete bridges using a LSTM recurrent neural network. *Structure and Infrastructure Engineering*, *19*(4), 475–489. https://doi.org/10.1080/15732479.2021.1951778

[23] Jia, J., & Li, Y. (2023). Deep learning for structural health monitoring: Data, algorithms, applications, challenges, and trends. *Sensors*, *23*(21), 8824. https://doi.org/10.3390/s23218824

[24] Sharma, S., & Sen, S. (2023). Real-time structural damage assessment using LSTM networks: Regression and classification approaches. *Neural Computing and Applications*, *35*(1), 557–572. https://doi.org/10.1007/s00521-022-07773-6

[25] Ba, P., Zhu, S., Chai, H., Liu, C., Wu, P., & Qi, L. (2024). Structural monitoring data repair based on a long short-term memory neural network. *Scientific Reports*, *14*(1), 9974. https://doi.org/10.1038/s41598-024-60196-2

[26] Hochreiter, S., & Schmidhuber, J. (1997). Long short-term memory. *Neural Computation*, *9*(8), 1735–1780. https://doi.org/10.1162/neco.1997.9.8.1735

[27] Elman, J. L. (1990). Finding structure in time. *Cognitive Science*, *14*(2), 179–211. https://doi.org/10.1207/s15516709cog1402_1

[28] Avci, O., Abdeljaber, O., Kiranyaz, S., Hussein, M., Gabbouj, M., & Inman, D. J. (2021). A review of vibration-based damage detection in civil structures: From traditional methods to Machine Learning and Deep Learning applications. *Mechanical Systems and Signal Processing*, *147*, 107077. https://doi.org/10.1016/j.ymssp.2020.107077

[29] Zhang, H., Wang, L., & Shi, W. (2023). Seismic control of adaptive variable stiffness intelligent structures using fuzzy control strategy combined with LSTM. *Journal of Building Engineering*, *78*, 107549. https://doi.org/10.1016/j.jobe.2023.107549

[30] Liu, Z., Shi, G., & Liu, Y. (2025). A novel approach to analyzing the mechanical response of component failure in cable truss structures using an improved LSTM neural network. *Engineering Failure Analysis*, *174*, 109532. https://doi.org/10.1016/j.engfailanal.2025.109532

[31] Smailov, N., Tolemanova, A., Ayapbergenova, A., Tashtay, Y., & Amir, A. (2025). Modelling and application of fibre optic sensors for concrete structures: A literature review. *Civil Engineering and Architecture*, *13*(3), 1885–1897. https://doi.org/10.13189/cea.2025.130332

[32] Zabihollah, A., & Shi, Y. (2025). Reliability analysis of residential buildings under hurricane using embedded FBG sensors: Remaining useful lifetime analysis. *Journal of Optics and Photonics Research. Advance online publication*. https://doi.org/10.47852/bonviewJOPR52024397

[33] Reddy, J. N. (2005). *An introduction to the finite element method*. McGraw Hill.

[34] Sarkandi, G. I., & Zabihollah, A. (2011). A computational model for health monitoring of storage tanks using fiber Bragg grating optical fiber. *Journal of Civil Structural Health Monitoring*, *1*(3–4), 97–102. https://doi.org/10.1007/s13349-011-0010-z

[35] Mehta, K. C., & Coulbourne, W. L. (2010). *Wind loads: Guide to the wind load provisions of ASCE 7-05*. American Society of Civil Engineers. https://doi.org/10.1061/9780784408582

How to Cite: Shi, Y., Zabihollah, A., Yu, Y-C., Pathak, A., & Oyetunji, O. (2025). Remaining Life Estimation of Power Towers Using Strain Sensor Data and LSTM Sequence to Sequence Models. *Journal of Optics and Photonics Research*. https://doi.org/10.47852/bonviewJOPR52026594

Appendix

For a two-dimensional frame structure, the element matricesre expressed as:

$$[K]=\frac{EI}{l}\begin{bmatrix} \frac{A}{I} & 0 & 0 & -\frac{A}{I} & 0 & 0 \\ 0 & \frac{12}{l^2} & \frac{6}{l} & 0 & -\frac{12}{l^2} & \frac{6}{l} \\ 0 & \frac{6}{l} & 4 & 0 & -\frac{6}{l} & 2 \\ -\frac{A}{I} & 0 & 0 & \frac{A}{I} & 0 & 0 \\ 0 & -\frac{12}{l^2} & -\frac{6}{l} & 0 & \frac{6}{l} & -\frac{6}{l} \\ 0 & \frac{6}{l} & 2 & 0 & -\frac{6}{l} & 4 \end{bmatrix},\ [\boldsymbol{M}]=\frac{\rho Al}{420}\begin{bmatrix} 140 & 0 & 0 & 70 & 0 & 0 \\ 0 & 156 & 22l & 0 & 54 & -13l \\ 0 & 22l & 4l^2 & 0 & 13l & -3l^2 \\ 70 & 0 & 0 & 140 & 0 & 0 \\ 0 & 54 & 13l & 0 & 156 & -22l \\ 0 & -13l & -3l^2 & 0 & -22l & 4l^2 \end{bmatrix}$$

where ρ is the mass density of the element, A is the cross-sectional area of the element, l is the element, and I_z is the moment of inertia of the cross-section of the beam concerning the z-axis, and E is Young's modulus of the element. For details on finite element procedure, one may consult the book written by Reddy [33].